Title

Non-invasive in vivo assessment of IDH1 mutational status in glioma

Journal

Nature Communications, 4(1)

ISSN

2041-1723

Authors

Chaumeil, Myriam M

Larson, Peder EZ

Yoshihara, Hikari AI

et al.

Publication Date

2013

DOI

10.1038/ncomms3429

Peer reviewed

Published in final edited form as:
Nat Commun. 2013 ; 4: 2429. doi:10.1038/ncomms3429.

Non-invasive *in vivo* assessment of IDH1 mutational status in glioma

Myriam M. Chaumeil[1], **Peder E.Z. Larson**[1], **Hikari A.I. Yoshihara**[1], **Olivia M. Danforth**[1], **Daniel B. Vigneron**[1], **Sarah J. Nelson**[1,2], **Russell O. Pieper**[2,3], **Joanna J. Phillips**[2,3,4], and **Sabrina M. Ronen**[1,2]

[1]Department of Radiology and Biomedical Imaging, University of California San Francisco, 1700 4th Street San Francisco 94158, CA, USA

[2]Brain Tumor Research Center, University of California San Francisco, San Francisco, CA 94143, CA, USA

[3]Department of Neurological Surgery, Helen Diller Research center, University of California San Francisco, San Francisco, CA 94143, CA, USA

[4]Department of Pathology, University of California San Francisco, San Francisco, CA 94143, CA, USA

Abstract

Gain-of-function mutations of the isocitrate dehydrogenase 1 (IDH1) gene are among the most prevalent in low-grade gliomas and secondary glioblastoma. They lead to intracellular accumulation of the oncometabolite 2-hydroxyglutarate, represent an early pathogenic event, and are considered a therapeutic target. In this proof-of-concept study, we show that [1-^{13}C] α-ketoglutarate can serve as a metabolic imaging agent for non-invasive, real-time, *in vivo* monitoring of mutant IDH1 activity, and can inform on IDH1 status. Using ^{13}C magnetic resonance spectroscopy in combination with dissolution Dynamic Nuclear Polarization, the metabolic fate of hyperpolarized [1-^{13}C] α-ketoglutarate is studied in isogenic glioblastoma cells that differ only in their IDH1 status. In lysates and tumors that express wild-type IDH1, only hyperpolarized [1-^{13}C] α-ketoglutarate can be detected. In contrast, in cells that express mutant IDH1, hyperpolarized [1-^{13}C] 2-hydroxyglutarate is also observed, both in cell lysates and *in vivo* in orthotopic tumors.

INTRODUCTION

Genetic screening has determined that over 70% of low-grade diffuse glioma tumors, and up to 90% of secondary glioblastoma (GBM) cases harbor a missense point mutation in one copy of the gene encoding for the cytosolic isocitrate dehydrogenase 1 (IDH1) enzyme, most commonly at residue 132 [1,2]. Mutations in an equivalent residue of the mitochondrial isoform isocitrate dehydrogenase 2 (IDH2) have also been reported in about 20% of acute lymphoblastic leukemia [3]. More recently, similar mutations have been observed in other

Corresponding author: Sabrina M. Ronen, Ph.D., 1700 4th Street, Box 2532, Byers Hall 3rd Floor, Suite, University of California, San Francisco, San Francisco, CA 94158, sabrina.ronen ucsf.edu, Phone: 415-514-4839, Fax: 415-514-2550.

AUTHOR CONTRIBUTIONS

M.M.C. designed and performed the experiments and wrote the paper. P.E.Z.L, J.J.P. and H.A.I.Y designed and performed experiments and contributed to writing the paper. O.M.D. performed experiments. D.B.V., S.J.N., R.O.P. designed experiments and reviewed the paper. S.M.R. conceived the study, designed the experiments, and wrote the paper.

CONFLICT OF INTEREST

The authors have no conflict of interest to declare.

cancers, including thyroid carcinomas (16%), cartilaginous tumors (75%) and intrahepatic cholangiocarcinomas (10% to 23%) [4].

The role and significance of mutant and wild-type IDH1 in cancer have been studied by several groups (see recent reviews [5,6]). Reports from clinical samples demonstrate that IDH1 mutations are monoallelic, with one copy of the wild-type gene and one copy of the mutant gene expressed in human tumors [7]. Whereas wild-type IDH1 catalyzes the oxidation of isocitrate to alpha-ketoglutarate (α-KG, 2-oxoglutarate), the mutant IDH1 isoform reduces α-KG to 2-hydroxyglutarate (2-HG), resulting in 2-HG levels that are 10–100 times greater than in wild-type tissue [1,2]. The interaction between wild-type and mutant enzymes is still under investigation [8,9]; however, it is well established that the presence of mutant IDH1 and elevated 2-HG leads to inhibition of α-KG-dependent dioxygenases, including histone demethylases and the TET family of 5-methylcytosine hydroxylases. This, in turn, leads to genome-wide changes in histone and DNA methylation [10,11]. The IDH1 mutation is thus an early oncogenic event that mediates tumor development through reorganization of the methylome and transcriptome [12,13]. In light of its critical role in tumor pathogenesis, drugs that target mutant IDH1 are now under development[14,15].

In this context, non-invasive methods for real-time monitoring of IDH1 activity and modulation of 2-HG production would be valuable for tumor characterization, patient stratification and prognosis, as well as optimization of mutant IDH1 inhibitors, and subsequent longitudinal monitoring of IDH1-targeted treatments. ^{1}H magnetic resonance spectroscopy (MRS) is a non-invasive imaging method that can probe steady-state metabolite levels. It has been used as a diagnostic and prognostic tool in brain tumor patients [16,17] and is able to detect the presence of 2-HG in glioma patients *in vivo* [18–21], in preclinical rodent models [22,23] and in biopsy samples [24,25]. An alternative, and potentially complementary, metabolic neuroimaging approach is ^{13}C MRS. This technique informs on real-time metabolic fluxes by probing the fate of exogenous ^{13}C-labeled substrates. The recent development of dissolution Dynamic Nuclear Polarization (DNP) has allowed ^{13}C-labeled compounds to be hyperpolarized, dissolved into solution, and injected into the sample of interest, to provide a 10,000 to 50,000-fold increase in signal-to-noise ratio (SNR) compared to thermally polarized compounds [26]. ^{13}C MRS of hyperpolarized compounds can thus be applied to monitor *in vivo* enzymatic activities [27]. The conversion of hyperpolarized [1-^{13}C] pyruvate to [1-^{13}C] lactate has been used to detect the presence of tumor and response to treatment in several pre-clinical models of cancer [27,28], including glioma [29–32]. These promising findings led to the first Phase I clinical trial of this technology, which was recently completed at the University of California, San Francisco [27,33]. It clearly demonstrated the translational value of this approach by detecting elevated ratios of hyperpolarized lactate-to-pyruvate in tumors of prostate cancer patients. In addition to pyruvate, a number of other hyperpolarized probes have been developed in order to monitor other metabolic pathways, measure pH, evaluate necrosis, assess redox potential, and measure vascular flow [27].

In this report, we demonstrate the successful use of a new DNP probe, [1-^{13}C] α-KG, for non-invasive ^{13}C MRS imaging of IDH1 status. We show that, following exposure to hyperpolarized [1-^{13}C] α-KG, we can detect the production of hyperpolarized [1-^{13}C] 2-HG in lysates and orthotopic tumors of cells engineered to express mutant IDH1, but not in lysates or tumors of their isogenic counterparts engineered to express wild-type IDH1, nor in normal contralateral brain. We conclude that [1-^{13}C] α-KG is a promising agent for the *in vivo* interrogation of IDH1 mutational status and activity.

RESULTS

Characterization of hyperpolarized α-ketoglutarate

To test the hypothesis that hyperpolarized [1-^{13}C] α-KG can serve as an imaging probe to monitor mutant IDH1 activity (Fig. 1a), we first determined its achievable polarization level and its T_1 relaxation time. [1-^{13}C] α-KG was mixed with a stable free radical in a 3:1 mixture of water and glycerol. After 1h, a polarization level of 16±3% was achieved in solution at 37°C (time constant τ=1381s). Following dissolution to an isotonic solution (pH=7.5±0.1, n=6), the resonances of hyperpolarized [1-^{13}C] α-KG ($\delta_{C1\text{-}\alpha KG}$=172.6ppm), [1-^{13}C] α-KG hydrate ($\delta_{\alpha KG\text{-}H}$ =180.9ppm) and [5-^{13}C] α-KG ($\delta_{C5\text{-}\alpha KG}$ =184 ppm, originating from the 1.1% natural abundance ^{13}C at the C5 position) were detected (Fig. 1b). The *in vitro* T_1 values of all three resonances were determined at 3 and 11.7 Tesla (Table 1). The *in vitro* T_1 values of hyperpolarized [1-^{13}C] 2-HG were determined separately (Table 1). Importantly, the lifetime of hyperpolarized [1-^{13}C] α-KG at 3 Tesla was sufficiently long (T_1=52±4s) that we expected to be able to probe α-KG metabolism at this field strength.

Studies in cell lysates

U87 GBM cells were transduced with a lentiviral vector coding, respectively, for wild-type IDH1 (U87IDHwt cells), or for mutant and wild-type IDH1 (U87IDHmut cells; recapitulating the monoallelic expression observed in patient samples [7]). Western blot analysis confirmed elevated mutant IDH1 protein in U87IDHmut cells, and elevated wild-type IDH1 in both cell lines (Fig. 2a and Supplementary Figure S1). A spectrophotometric assay confirmed the functionality of the expressed mutant IDH1 (Fig. 2b); the rate of NADPH consumption was almost six times higher in U87IDHmut than in U87IDHwt cells: $R^{U87IDHmut}$=0.64±0.06 versus $R^{U87IDHwt}$=0.13±0.06 fmol NADPH-consumed.min^{-1} per cell (P <0.01). Finally, 1D ^{1}H MRS (Fig. 2c) confirmed the presence of 2-HG in U87IDHmut cell lysates, with 2D ^{1}H MRS of the same lysates confirming the 2-HG assignment (Fig. 2d). The level of 2-HG U87IDHmut cells was 5.3±1.3 fmol.cell^{-1} or 10.1±2.5 μmol per gram assuming a cell diameter of ~10μm. 2-HG resonances were below detection level in wild-type cells.

To show that the conversion of α-KG to 2-HG can be detected within the hyperpolarization lifetime, we first probed the fate of hyperpolarized [1-^{13}C] α-KG in cell lysates. Following injection, a new resonance was detected at 183.9ppm in U87IDHmut but not in U87IDHwt cell extracts (Fig. 3a). This resonance was assigned to [1-^{13}C] 2-HG and the assignment further confirmed by 2D ^{1}H-^{13}C MRS (Fig. 3b.). Normalization to the [5-^{13}C] α-KG peak (the T_1 of which is comparable, see Table 1) indicated that 2-HG was accumulating over time (Fig. 3c; in addition to T_1 relaxation, the resonance of [5-^{13}C] α-KG also decreases due to conversion of α-KG to 2-HG leading to an ~2% overestimate of 2-HG production).

Studies in orthotopic tumors

Next, it was necessary to confirm that enough hyperpolarized [1-^{13}C] α-KG is delivered and metabolized to produce detectable amounts of [1-^{13}C] 2-HG *in vivo*, where [1-^{13}C] α-KG needs to be delivered to the brain, cross the blood brain barrier (BBB), penetrate the tumor, and permeate the cell membrane. To this end, orthotopic tumors were implanted in the right putamen of athymic rats [31]. When tumors reached 0.38±0.15cm^3, hyperpolarized [1-^{13}C] α-KG (v=2ml, c=100mM) was injected intravenously.

In a first experiment, dynamic ^{13}C spectra were acquired every 3s from an axial slab including the whole tumor (2cm thickness, Fig. 4a). Data were acquired from the beginning of the intravenous injection using a multi-band variable flip angle (*VFA)* excitation scheme optimized to monitor 2-HG production by preserving the α-KG hyperpolarization and

efficiently using the available magnetization to enhance the detection of 2-HG [34,35]. Hyperpolarized [1-^{13}C] α-KG, hyperpolarized [1-^{13}C] α-KG hydrate, and a resonance at 184ppm were detected (Fig. 4b). The amount of [1-^{13}C] α-KG in the slab was not significantly different between U87IDHwt and U87IDHmut animals, suggesting comparable delivery of the hyperpolarized substrate to the brain (Fig. 4c). Given the ≈ 1ppm linewidth of the 184ppm resonance *in vivo*, and in light of our findings in cell extracts showing that [5-^{13}C] α-KG and [1-^{13}C] 2-HG are only 0.1ppm apart, these two resonances could not be spectrally resolved. Nonetheless, we found a substantial difference in the temporal evolution of the 184ppm peak between mutant and wild-type IDH1 animals. In U87IDHwt animals, this resonance presents a unimodal temporal evolution centered around the time of maximum hyperpolarized [1-^{13}C] α-KG (approximately 10s post injection), and likely corresponds to the hyperpolarized [5-^{13}C] α-KG resonance originating from the injected solution (Fig. 4d). In contrast, the same resonance follows a bimodal temporal evolution in U87IDHmut animals, suggesting a delayed metabolic production of hyperpolarized [1-^{13}C] 2-HG, with a maximum around 20s (Fig. 4d).

We then examined the spatial distribution of hyperpolarized metabolites using a dedicated 2D ^{13}C chemical shift imaging (CSI) sequence [34,36,37]. Data were acquired from the beginning of the intravenous injection every 5s with an in-plane spatial resolution of 5mm. A multi-band excitation scheme was used to increase the signal of 2-HG by preserving the magnetization of its precursor α-KG [34].

The grid used for 2D CSI acquisition is shown as an overlay to a T2-weighted MR image for a U87IDHmut animal (Fig. 5a). Tumor volumes were not significantly different between U87IDHmut and U87IDHwt tumor-bearing animals ($Volume^{wt}$=0.38±0.19cm^3 versus $Volume^{mut}$=0.38±0.12cm^3, unpaired Student *t*-test: $p=0.7$). The levels of hyperpolarized [1-^{13}C] α-KG were measured in tumor voxels (red/blue, n=6, including n=3 U87IDHmut and n=3 U87IDHwt), in normal brain voxels (green, n=6), and in blood-containing voxels centered on the basal artery (orange, n=6) for each imaging time point (Fig. 5b). As expected, the levels of hyperpolarized [1-^{13}C] α-KG were significantly higher in blood-containing voxels as compared to normal brain (Unpaired Student *t*-test: $**p<0.005$ at 10, 15, 20 and 25s; $*p<0.05$ at 30s). In addition, significantly higher levels of hyperpolarized [1-^{13}C] α-KG were observed in the tumor voxels as compared to normal brain (Unpaired Student *t*-test: $**p<0.005$ at 10, 15, 20 and 25s; $*p<0.05$ at 30s), and no significant differences in hyperpolarized [1-^{13}C] α-KG levels were observed between tumor and blood-containing voxels, suggesting higher delivery and retention of hyperpolarized [1-^{13}C] α-KG in the tumor region. This effect is consistent with increased angiogenesis, elevated vascular permeability, and BBB breakdown in the tumor [31], and likely enhances our ability to detect α-KG metabolism within the tumor region. Importantly, hyperpolarized [1-^{13}C] α-KG levels were not significantly different between U87IDHwt and U87IDHmut tumors at any of the time points monitored (Fig. 5c), indicating that substrate delivery to tumor is independent of tumor IDH1 status, and is thus not a confounding factor in the detection of hyperpolarized [1-^{13}C] 2-HG.

Hyperpolarized ^{13}C MR spectra from one U87IDHwt tumor (blue), one U87IDHmut tumor (red), one normal brain (green), and one blood voxel (orange) show the temporal evolution of hyperpolarized metabolites (Fig. 5d). The 184ppm resonance was observed only in the mutant IDH1 tumor voxel and appeared only at 20s post injection (Fig. 5d). It was not observed in wild-type tumor or blood voxels, in spite of the comparable delivery of hyperpolarized [1-^{13}C] α-KG in these three voxel types. Based on this data, we attributed the 184ppm resonance observed at 20s in mutant IDH1 tumors to hyperpolarized [1-^{13}C] 2-HG. When considering all the rats studied (n=6), the SNR of hyperpolarized [1-^{13}C] 2-HG was $SNR^{mut}_{[1\text{-}^{13}C]\ 2\text{-}HG}$ =1.4±0.2 in U87IDHmut tumors, whereas the resonance of

hyperpolarized [1-^{13}C] 2-HG was not detectable in any of the U87IDHwt tumors at that time point ($SNR^{wt}_{[1\text{-}^{13}C]\ 2\text{-}HG}$ =1.0±0.1; Unpaired Student *t*-test: **p*<0.05, Fig. 5e). Consequently, although the SNR of hyperpolarized [1-^{13}C] 2-HG was low, our results demonstrate statistical significance in discriminating between mutant IDH1 and wild-type tumors.

This data also served to determine the *in vivo* effective decays of [1-^{13}C] α-KG in U87IDHwt animals, in which no metabolism of α-KG to 2-HG was expected. The measured decays were 17.7±1.8s in the vasculature and 20.6±1.7s in the normal brain. As expected, these *in vivo* values are shorter than the *in vitro* measurements, as these decays include losses of polarization due to T_1, flow, and potentially metabolism [38].

U87IDHwt and U87IDHmut tumors of comparable size are shown in Fig. 6a. Heatmaps illustrate high levels of hyperpolarized [1-^{13}C] α-KG in the blood vessels underneath the brain and in the tumors, regardless of tumor IDH1 status (Fig. 6b). In contrast, heatmaps of hyperpolarized [1-^{13}C] 2-HG show the presence of 2-HG in U87IDHmut tumor only; this resonance is absent from blood-rich areas underneath the brain, from normal brain voxels and from U87IDHwt tumors (Fig. 6c). Similar findings were made in all U87IDHmut (n=3) and U87IDHwt tumors (n=3).

Post-mortem analysis

Immunohistochemical staining confirmed the presence of the mutant IDH1 isoform in U87IDHmut tumors, but not in U87IDHwt (Fig. 7a). In line with these results, 2-HG was detectable using ^{1}H MRS only in the extracts of U87IDHmut tumors. The average level of 2-HG was 9.8±1.6 μmol per gram of tumor (n=3) and consistent with the estimated 10.1±2.5 μmol per gram in cell lysates (Fig. 7b).

DISCUSSION

Our results show that hyperpolarized [1-^{13}C] α-KG fulfills the mandatory requirements for a useful MR metabolic imaging probe. The T_1 relaxation time of [1-^{13}C] α-KG in solution at 3 Tesla (52s) compared favorably with the T_1 values of other commonly used DNP probes measured at 1.5–3 Tesla ([1-^{13}C] pyruvate: $T_1 \approx$ 45–60s [39]; [1-^{13}C] lactate: $T_1 \approx$ 45s [40]; [1-^{13}C] alanine: $T_1 \approx$ 40s [41]). The T_1 of such carbonyl-labeled DNP probes, including α-KG, is dominated by chemical shift anisotropy (*CSA*) relaxation processes. As a result, although lower magnetic fields lead to poorer spectral resolution, studies of hyperpolarized [1-^{13}C] α-KG, like other hyperpolarized probes, benefit from lower field strengths at which the *CSA* is minimized ($CSA\ \alpha\ B_0^2$) and the T_1 is longer.

The level of liquid state polarization (16% at 37°C) was also comparable to the values reported for other hyperpolarized ^{13}C-carbonyl-labeled probes (range 7–30%) [27]. Achieving this polarization level required dissolving [1-^{13}C] α-KG in a glassing agent (glycerol), at high concentration (5.9M), and optimizing the concentrations of free radical and gadolinium agent. As our results show, the polarization level achieved using a Hypersense™ DNP system provided sufficient SNR for detection of hyperpolarized [1-^{13}C] α-KG and its metabolic product, hyperpolarized [1-^{13}C] 2-HG, in an animal *in vivo*. Further enhancements in polarization level could be achieved thanks to newly developed equipment such as the GE SpinLab™ clinical polarizer, which has been shown to increase polarization levels through use of a lower temperature and higher magnetic field for DNP[42,43].

A potential limitation of our study is the model system, which was genetically engineered to express mutant IDH1. We chose this approach because no models of clinical origin were available when we initiated our study. In fact, to date, only one tumor-forming model of clinical origin has been described [44]. Importantly however, the levels of 2-HG detected in

our tumor extracts (9.8±1.6 μmol per gram of tumor) were comparable to the levels reported in patients (5 to 35 μmol of 2-HG per gram) [2] and studies of this model using ^{1}H MRS at high field strengths (7 and 14.1 Tesla) also detected 2-HG *in vivo* [22,23]. In light of these findings, we believe that the use of a genetically engineered model was justified for our proof-of-concept imaging study.

Following *in vitro* injection of hyperpolarized [1-^{13}C] α-KG into cell lysates, hyperpolarized [1-^{13}C] 2-HG at 183.9ppm could be detected in U87IDHmut but not in U87IDHwt lysates. After intravenous injection, hyperpolarized [1-^{13}C] α-KG was also detected *in situ* in orthotopic tumors, indicating that the probe was delivered to the brain and crossed the BBB in the tumor region. Some reports suggest that α-KG does not easily permeate the cell membrane [45], while other studies show that brain cells are capable of taking up extracellular α-KG [46]. Our results demonstrate that, at least in our model, enough hyperpolarized [1-^{13}C] α-KG permeates the tumor cells *in vivo* to enable the detection of its conversion to hyperpolarized [1-^{13}C] 2-HG within a time frame compatible with a hyperpolarized ^{13}C MRS experiment. Furthermore, our approach can serve to distinguish between mutant IDH1 and wild-type IDH1 tumors *in vivo*.

Improvements in the delivery of hyperpolarized [1-^{13}C] α-KG, as well as in the detection of hyperpolarized [1-^{13}C] 2-HG, could be achieved by using alternative α-KG-based DNP probes. In particular, ester derivatives of α-KG, including octyl- and fluorobenzyl-esters have been reported to permeate the cell membrane more effectively [45]. Such derivatives would lead to increased intracellular α-KG concentrations and potentially higher levels of 2-HG, and might also enable studies of IDH2 within the mitochondria [46,47]. Previous studies indicate that the use of ester derivatives creates additional resonances than could hamper spectral differentiation [48]. However, preliminary studies in our lab investigating [1-^{13}C] dimethyl-α-KG show that the compound resonates far from our spectral region of interest, and thus would not hamper 2-HG detection. Furthermore, the natural abundance [5-^{13}C] resonance of the ester was not detectable in our preliminary data, and, if present, would also be expected to resonate away from [1-^{13}C] 2-HG.

Our studies were enhanced by the use of innovative *VFA* and multi-band ^{13}C MR pulse sequences, which use the α-KG polarization efficiently while maximizing the signal of [1-^{13}C] 2-HG and minimizing the signal from [5-^{13}C] α-KG [34–37]. Specifically, [5-^{13}C] α-KG originates from the injected hyperpolarized solution and is consequently present at early time points. In contrast, [1-^{13}C] 2-HG is produced metabolically, and thus builds up at later time points. In our study, the multi-band sequence preserved the magnetization of [1-^{13}C] α-KG by using a relatively low flip angle (*FA)* for its frequency, but quenched the polarization of [5-^{13}C] α-KG at the early time points by using a higher *FA* in that region. Furthermore, the *VFA* scheme enhanced the signal of [1-^{13}C] 2-HG at the later time points by increasing the *FA* over time. The use of such sequences is critical for enabling the direct detection of hyperpolarized [1-^{13}C] 2-HG *in vivo*.

When considering the possibility of future clinical translation, the dose of hyperpolarized α-KG needs to be considered. In the case of hyperpolarized pyruvate, the Phase I clinical trial recently completed at UCSF [33] was based on a large number of animal studies in which 2ml of 80mM hyperpolarized pyruvate (~10mL.kg^{-1}, 0.8mmoles of pyruvate per kg) was injected in rats [49], and a comparable dose of 0.3ml of 80mM (~10mL.kg^{-1}, 0.8mmoles of pyruvate per kg) was used in over 200 studies in mice, all with no adverse effects. In the clinical trial, the rodent studies were scaled in patients to a dose of 0.42ml/kg of 250mM pyruvate (0.1mmoles of pyruvate per kg). Thus, volumes of 30–40 ml were injected, representing 1% of the Total Blood Volume (TBV). These doses were very well tolerated with no dose-limiting toxicities, and resulted in highly significant imaging results with a

spatial resolution as low as 1cm isotropic. In the case of α-KG, the concentration of hyperpolarized compound in our studies was limited by the technical requirements of the Hypersense™ hyperpolarizer (maximum volumes of substrate and dissolution buffer) resulting in a maximum achievable concentration of injected α-KG of 100mM. However, the dose of α-KG used in this study (0.1g.kg^{-1} body weight) was 6.8 times lower (for a 200g rat) than the No Observed Adverse Effect Level reported in rodents (NOAEL=1g.kg^{-1} body weight) [50], and α-KG is sold in the United States as an over-the-counter nutritional supplement. Consistent with these facts, no adverse effects were observed in any of the animals included in our study (n=11), and higher levels of α-KG could potentially be injected. However, as in the case of pyruvate, the concentration of α-KG would need to be increased in order to perform a similar study in patients with acceptable injections volumes.

Recent studies demonstrate that total 2-HG levels can be monitored *in vivo* using 1D or 2D ^{1}H MRS in patients at clinical field strengths (1.5–3 Tesla) [18–21]. In an effort to compare ^{1}H MRS with our hyperpolarized ^{13}C approach for a potential clinical study, we performed an additional experiment, in which we compared the sensitivity of our rodent coil with the sensitivity of a ^{13}C human head coil array. The sensitivity of the human coil was lower by a factor of ~9. However, reported ^{1}H MRS studies were performed in voxel sizes of either 8cm^3 i.e. ~16 times larger than our study (no SNR reported in post processed data) [19,20] or 27cm^3 i.e. ~54 times larger than our study (SNR=5) [18]. With such voxel sizes we estimate that we would achieve, respectively, an SNR of ~2.5 and an SNR of ~8.4 on hyperpolarized [1-^{13}C] 2-HG.

Nonetheless, before clinical translation can be achieved, the approach presented in this proof-of-concept study will likely require further optimization to enhance [1-^{13}C] 2-HG detection. Several areas of improvement can be envisaged. As mentioned above, the SpinLab clinical polarizer has been shown to enhance the achievable polarization levels [42,43]. This would increase the SNR of our hyperpolarized species, lead to better time-resolved kinetics, and thus improve the detection of [1-^{13}C] 2-HG. Higher concentrations of [1-^{13}C] α-KG, or a more BBB and cell-permeable derivative of α-KG, could result in increased amounts of [1-^{13}C] α-KG delivered to the tumor and, in turn, greater production of [1-^{13}C] 2-HG (until the IDH1 enzyme is saturated). Finally, pulse sequences that would enhance the SNR of hyperpolarized [1-^{13}C] 2-HG can be implemented. A non-dynamic 2D CSI sequence with a 90-degree *FA* at 20 seconds post injection would generate a higher SNR by a factor of ~3 compared to our current study, albeit at the detriment of temporal information. More promising is the recently developed 2D CSI sequence combining the multiband and *VFA* scheme [35], which would enhance the signal of [1-^{13}C] 2-HG by using a progressively increasing *FA*. In addition, ^{1}H decoupling could be implemented to further increase the *in vivo* SNR of [1-^{13}C] 2-HG, as previously reported [51].

Importantly, the information obtained by ^{13}C MRS is somewhat different from that obtained by ^{1}H MRS. ^{1}H MRS detects the total, steady-state, 2-HG levels present in both the extracellular and intracellular compartments [2]. In contrast, ^{13}C MRS dynamically informs on the metabolic fate of hyperpolarized [1-^{13}C] α-KG. Accordingly, although we cannot rule out some residual enzymatic activity in necrotic regions [52, ^{13}C MRS primarily probes the enzymatic activity of mutant IDH1 in live, metabolically active cells, and, as such, can inform in real-time on the presence of active mutant IDH1, 2-HG synthesis, and its potential inhibition by novel therapies [14,15].

In summary, in this proof-of-concept study, we used ^{13}C MRS and were able to monitor the conversion of hyperpolarized [1-^{13}C] α-KG into hyperpolarized [1-^{13}C] 2-HG in cell lysates and, more importantly, *in vivo* in orthotopic brain tumors. Hyperpolarized [1-^{13}C] α-KG presents a promising, non-radioactive and potentially clinically relevant agent for

interrogation of IDH1 status *in vivo*. This innovative method provides information on IDH1 mutational status and activity *in situ*, it informs on real-time 2-HG production and complements the ^{1}H MRS methods that detect total steady-state 2-HG levels [18–20]. Additional optimization is required prior to clinical translation. Nonetheless, ^{13}C MRS of hyperpolarized [1-^{13}C] α-KG could ultimately provide an additional valuable tool for diagnosis, prognosis, patient stratification, drug development and studies of response to emerging mutant IDH1-targeted therapies.

METHODS

Hyperpolarization of α-ketoglutarate

[1-^{13}C] α-ketoglutaric acid (2-oxoglutaric acid, Sigma Aldrich, St Louis, MO) was dissolved in a mixture of water and glycerol (3:1 in volume), with 17.3mM of OX63 trityl radical and 0.4mM of Dotarem (Guerbet, France), to a final concentration of 5.9M. A volume of 6.4μL (cell lysate experiments) or 53μL (*in vivo* experiments) was polarized using a Hypersense™ polarizer (Oxford Instruments, Oxfordshire, UK) for approximately 1h (3.35 Tesla, 1.4K, 94.089GHz). Following polarization, hyperpolarized [1-^{13}C] α-KG was rapidly dissolved in a Tris-based isotonic buffer (pH=7.5±0.1) and used in this form for all experiments.

Relaxation times and polarization levels

A volume of 20μL of [1-^{13}C] α-KG was polarized as described above. Immediately after dissolution in an isotonic Tris-based buffer (40mM Tris, 80mM NaOH, 0.1mg.L^{-1} Na_2EDTA) to obtain a 40mM solution buffered at physiological pH, hyperpolarized [1-^{13}C] α-KG was placed in a 5mL syringe (n=3, 3 Tesla Signa clinical MR system, GE Healthcare, Waukesha, WI) or in a 10mm NMR tube (n=3, 11.7 Tesla INOVA spectrometer, Agilent Technologies, Inc., Palo Alto, CA) and ^{13}C spectra were acquired using a 5-degree flip angle (*FA)* and a repetition time TR=3s (Parameters at 3 Tesla: Number of Transients NT=64, spectral width SW=5kHz, 2048points; Parameters at 11.7 Tesla: NT=300, SW=20kHz, 4000points). For each field strength, the T_1 relaxation times of hyperpolarized [1-^{13}C] α-KG ($\delta_{C1\text{-}\alpha KG}$ =172.6ppm), hyperpolarized [1-^{13}C] α-KG hydrate ($\delta_{\alpha KG\text{-}H}$ =180.9ppm) and hyperpolarized [5-^{13}C] α-KG ($\delta_{C5\text{-}\alpha KG}$=184ppm) were determined by performing a monoexponential fit to the signal decay curve of the hyperpolarized compound [53].

Following complete decay of the hyperpolarized signal, a thermal spectrum with nearly identical parameters was acquired at 3 Tesla using a 90-degree *FA* and a repetition time of greater than 4xT_1 (TR=10 s, NT=64, T_1 of solution shortened by adding 50μL of Magnevist® (Bayer Healthcare, Shawnee Mission, KS) to the hyperpolarized solution). The level of polarization in solution was calculated by comparing the first hyperpolarized spectrum with its corresponding thermal spectrum, correcting for *FA* and number of scans. The amplitude of the hyperpolarized signal was also corrected for T_1 relaxation during the transfer time from the polarizer to the spectrometer (approximately 20s).

In order to evaluate the relaxation time T_1 of [1-^{13}C] 2-HG, unlabeled L-2-hydroxyglutaric acid (Sigma Aldrich, St Louis, MO) was dissolved in a mixture of water and glycerol (6:1 in volume), together with 17.3mM of OX63 trityl radical and 0.4mM of Dotarem (Guerbet, France). A volume of 100μL was polarized using the Hypersense polarizer using the same conditions as for [1-^{13}C] α-KG. After dissolution in 4mL of Tris-based buffer (final pH=7.6), ^{13}C MR spectra of hyperpolarized 2-HG were recorded using the same parameters as the ones used for α-KG, except that the *FA* was 10-degree instead of 5. Even though the compound was not ^{13}C-enriched on the C1 position, the 1.1% natural abundance of ^{13}C was

sufficient to generate a detectable hyperpolarized resonance at 183.9ppm. The relaxation time T_1 of [1-^{13}C] 2-HG at 3 Tesla and 11.7 Tesla was calculated as described above.

Cell models

Wild-type human IDH1 cDNA (MHS1010-58017, Open Biosytems, ThermoScientific) was mutagenized to generate an R132H-encoding cDNA using site-directed mutagenesis (Quick Change II, Applied Biosystems). Wild-type and mutant IDH1 cDNAs were then sub-cloned into separate green fluorescent protein (GFP)-encoding lentiviral expression vectors. U87 GBM cells were obtained from the American Tissue Culture Collection and cells expressing exogenous wild-type or mutant IDH1 were created by introduction of lentiviral constructs encoding either the wild-type (U87IDHwt) or R132H IDH1 (U87IDHmut) cDNA, followed by selection of GFP+ cells by flow cytometry and verification for expression of the wild-type or mutant proteins by Western blot using wild-type or R132H IDH specific antibodies. Both modified U87 strains were cultured under standard conditions in high glucose Dulbecco's Modified Eagle Medium (DMEM H-21, UCSF Cell Culture Facility, San Francisco, CA) supplemented with 10% heat-inactivated fetal bovine serum (Thermo Scientific Hyclone, Logan, UT), 2mM L-Glutamine (Invitrogen, Carlsbad, CA), 100u.mL^{-1} penicillin, and 100mg.mL^{-1} streptomycin (UCSF Cell Culture Facility). All cell lines in culture were maintained as exponentially growing monolayers at 37°C in a humidified atmosphere of 95% air and 5% CO_2.

Western blotting

Western blot analysis was performed on U87IDHmut and U87IDHwt cell lines to monitor IDH1 protein levels. Cytoplasmic proteins were electrophoresed on NuPAGE Novex 4–12% Bis-Tris gels (Life Technologies, Grand Island, NY) using the SDS-PAGE method and electrotransferred onto PVDF membranes. Blots were blocked and incubated with primary antibodies anti-IDH1wt (rabbit, #3997, 1:1000 dilution overnight, Cell Signaling Technology, Danvers MA) and anti-IDH1^{R132H} (mouse monoclonal H09 clone, 1:1000 dilution overnight, Dianova, Miami, FL), and then incubated with secondary antibody either anti-rabbit IgG (DyLight 800, 1:2000, Cell Signaling Technology, Danvers, MA) or anti-mouse IgG (DyLight 680, 1:2000, Cell Signaling Technology, Danvers, MA). The blots were visualized with a LI-COR Odyssey Infrared Imaging System (LI-COR Biosciences, Lincoln, NE).

Spectrophotometric assay

Mutant IDH1 activity was monitored in U87IDHmut and U87IDHwt cell lysates by adapting a spectrophotometric assay. For each cell type, ~2.0×10^7 cells were lysed in 400μL of 50mM Tris-based buffer with 1μl.mL^{-1} protease inhibitor cocktail (Sigma-Aldrich, St. Louis, MO). Lysates were then homogenized by passing through a 27Gauge needle and sonicated on ice at 10% amplitude (3×5s with 10s intervals) using an FB505 20kHz ultrasonicator (Fisher, Pittsburgh, PA). Cell lysates were centrifuged at 14,000rpm for 30min at 4°C. The supernatant was added to 1mL of reaction buffer composed of 33mM Tris-based buffer, 0.33mM EDTA, 0.1mM NADPH, 1.33mM $MnCl_2$, and 1.3mM α-KG (Sigma-Aldrich, St. Louis, MO). A volume of 100μL per well was then placed in a 96-well plate (Greiner Bio One, Monroe, NC). Absorbance at λ=340nm was monitored every 10s for 30min using an Infinite m200 spectrophotometer (Tecan Systems, Inc, CA) and correlated to the concentration of NADPH [54,55] using a previously established calibration curve. For each lysate, the reaction rate R_{IDHmut} of mutant IDH was calculated by linear regression of the first 300s and reported in fmol of NADPH-consumed.min^{-1} per cell (n=3 per cell type).

^{1}H MRS of in cell lysates

~1.5×10^{8} U87IDHmut and U87IDHwt cells were extracted using the dual-phase extraction method [29]. 1D ^{1}H MRS spectra of U87IDHmut (n=3) and U87IDHwt (n=3) extracts were acquired on a 14 Tesla spectrometer (Bruker BioSpin Corporation, Billerica, MA) equipped with a 5-mm broadband probe. For 1D ^{1}H MRS, the following acquisition parameters were used: 90-degree *FA*, Repetition time TR=2s, Spectral Width SW=7194Hz, 20000points, Number of transients NT=100. All spectral assignments were based on literature reports (www.hmdb.ca) and confirmed by 2D ^{1}H MRS (2D Total Correlation Spectroscopy (TOCSY) sequence; f2: SW=20000Hz, 8192points; f1: SW=6500Hz, 64points; mixing time 40ms, WURST-8 adiabatic spin lock). 2-HG levels were quantified by peak deconvolution and integration using ACD/SpecManager™ 9 (Advanced Chemistry Development, Toronto, Canada), correction for saturation and normalization to a TSP reference and to cell number (Cambridge Isotope Laboratories, Andover, MA).

Hyperpolarized ^{13}C MR studies of cell lysates

1.2×10^{8} U87IDHmut (n=3) and U87IDHwt (n=3) cells were extracted as described above. Lysates were placed in a 10mm NMR tube and combined with a reaction buffer of similar composition to that used in the IDH1 spectrophotometric enzyme assay (while maintaining the same substrate concentrations per cell). Additionally, $MgCl_2$ was used instead of $MnCl_2$ to prevent Mn^{2+}-induced paramagnetic relaxation of nuclear hyperpolarization. Within 10s of combining lysates and buffer, 1.2mL of hyperpolarized [1-^{13}C] α-KG dissolved in buffer (40mM Tris, 9.4mM NaOH, 0.1mg.L^{-1} Na_2EDTA) was added to a final concentration of 4.7mM. Immediately after injection, dynamic sets of hyperpolarized ^{13}C spectra were acquired on a 11.7 Tesla INOVA spectrometer (Agilent Technologies, Inc., Palo Alto, CA) with a 13-degree *FA* for 300s (TR=3s, NT=100, SW=20kHz, 40000points). After the total decay of the hyperpolarized signal, a 2D ^{1}H-^{13}C gradient-selected Heteronuclear Multiple Bond Coherence (gHMBC) spectrum of U87IDHmut cell lysate was recorded on a 14 Tesla Varian INOVA spectrometer (Agilent Technologies, Inc., Palo Alto, CA) equipped with a 5-mm cryogenically cooled triple resonance inverse probe in order to confirm the [1-^{13}C] 2-HG assignment: f2: SW=6903Hz, 2048points; f1: SW=36207Hz, 4000points. ^{13}C pulse delays were 3.75ms (to filter out one-bond coupling of 140Hz) and 100ms (optimal for 5Hz ^{1}H-^{13}C interactions).

Tumor-bearing animals

All animal research was approved by the Institutional Animal Care and Use Committee of the University of California, San Francisco. Athymic rats (n=6 U87IDHmut, n=5 U87IDHwt, average weight 200g, male, rnu/rnu homozygous, 5 to 6 week-old at the time of intracranial injection; Harlan Laboratories, Indianapolis, IN) were used in this study. An hour before starting the intracranial injection, U87IDHwt or U87IDHmut cells were washed once with phosphate buffered saline solution, harvested by trypsinization, counted and resuspended in serum-free McCoy's medium to a final concentration of 3×10^{5} cells per 10μL. For intracranial injection, rats were anesthetized by an intraperitoneal injection of a mixture of ketamine/xylazine (100/20mg.kg^{-1} respectively). A volume of 10μL of cell suspension was slowly injected into the right putamen of the animal brain by free hand technique [56]. Buprenorphine (dose=0.03mg.kg^{-1}, V=600μL) and bupivacaine (dose=5mg.kg^{-1}, v=300μL) were injected subcutaneously right before injection of tumor cells for optimal pain management.

In vivo hyperpolarized ^{13}C MR studies

In vivo experiments were performed on a 3 Tesla clinical MR system (GE Healthcare, WI) equipped with a dual-tuned ^{1}H-^{13}C transmit/receive volume coil ($Ø_I$=40mm). Rats were

anesthetized using isoflurane (1–2% in O_2, 1.5L.min^{-1}) and a 23Gauge catheter was secured in the tail vein for injection of hyperpolarized material.

Anatomical imaging was performed to assess tumor location (2D Fast Spin Echo (FSE), axial/coronal, TE/TR=20/1200ms, Field Of View (FOV)=40×40mm, matrix 256×256, 20slices, thickness=1mm, acquisition time 5min7s, NT=1). After 1h, hyperpolarized [1-^{13}C] α-KG was rapidly dissolved in isotonic buffer (40mM Tris, 200mM NaOH, 0.1mg.L^{-1} Na_2EDTA) to obtain a 100mM solution. Intravenous injection began within less than 20s after dissolution. A volume of 2mL of the hyperpolarized solution was injected over 12s.

Dynamic ^{13}C MR spectra were acquired from a 2cm slab including the whole tumor on U87IDHwt (n=2) and U87IDHmut (n=3) tumor-bearing animals. The custom radiofrequency (RF) pulses were limited to this thickness by the demanding spectral and spatial selection requirements combined with gradient and RF hardware limitations of the clinical scanner. Nonetheless, this slice thickness provided full coverage for all tumors, which usually had an ellipsoid shape and grew preferentially along the anterior-posterior direction. The slab was positioned to minimize the contributions of neck and nose blood vessels. Data were acquired using an adiabatic double spin-echo sequence (TE/TR=35/3000ms) [36]. It used multi-band spectral-spatial RF excitation pulses with a variable flip angle (*VFA*) scheme that started with a smaller flip angle (*FA)* for [1-^{13}C] α-KG (3.5-degree, *VFA1*) to preserve substrate magnetization and a larger *FA* for [1-^{13}C] 2-HG / [5-^{13}C] α-KG / [1-^{13}C] α-KG-hydrate (42.3-degree, *VFA2*) for improved SNR of 2-HG [34]. These *FAs* were progressively increased over time to efficiently use the hyperpolarized magnetization in the presence of metabolic conversion, with both *VFA1* and *VFA2* ramping up to a final 90-degree *FA* [35]. *FA* and frequency calibration was performed on a 0.6mL syringe of 8M [1-^{13}C] urea placed next to the head.

^{13}C 2D dynamic CSI was acquired starting 5s after the beginning of hyperpolarized [1-^{13}C] α-KG injection in U87IDHwt (n=3) and U87IDHmut (n=3) animals using a sequence optimized for α-KG/2-HG [34,37]. This optimization included using a specialized multiband spectral-spatial RF excitation pulse designed to provide a 4-degree *FA* for [1-^{13}C] α-KG (to preserve substrate magnetization) and 25-degree elsewhere for improved SNR for 2-HG. An echo-planar spectroscopic imaging (EPSI) readout gradient was used for increased imaging speed. This improves the SNR by reducing artifacts from T_1 decay, metabolic conversion, and motion that can cause signal loss and blurring. The EPSI was optimized for maximum SNR efficiency while meeting the spectral bandwidth and spatial resolution requirements. Additional sequence parameters were: adiabatic double spin-echo acquisition, bandwidth 543Hz, resolution 10.4Hz, 52points, TE/TR=140/215ms, matrix 8×18, 5×5mm resolution, slice thickness 2cm, 1.7s per image, images every 5s.

For all *in vivo* studies, B_0 shimming was performed using the automatic GE shimming routine, which acquires three orthogonal field maps and uses a least squares fit to set the linear shim gradients. The linewidth of [1-^{13}C] α-KG was 26.3±9.8Hz for the 1D MRS experiment (entire slab) and 23.0±3.4Hz for the 2D CSI (brain voxel). ^{1}H decoupling was not applied, however, its use could increase the *in vivo* SNR of [1-^{13}C] 2-HG in future studies, as illustrated by Marjanska *et al.* [51].

In vivo MR data analysis

Tumor volume was assessed from the anatomical T2-weighted images using the dedicated in-house SIVIC software (http://sourceforge.net/projects/sivic/). For each animal, manual contouring of the tumor was performed for all axial slices and linear extrapolation was used to estimate final tumor volume.

For *in vivo* slab dynamic experiments, integrals of hyperpolarized [1-^{13}C] α-KG and [1-^{13}C] 2-HG were quantified by peak integration of the dynamic hyperpolarized ^{13}C spectra using ACD/SpecManager™ 9 (Advanced Chemistry Development, Toronto, Ontario, Canada). The integrals were then corrected for the *VFA* schemes using Matlab® (Mathworks, Natick, MA).

For *in vivo* 2D CSI experiments, ^{13}C datasets were processed using SIVIC software to calculate the integrals of hyperpolarized [1-^{13}C] α-KG and [1-^{13}C] 2-HG, and the standard deviation of the noise to derive each metabolite SNR value. Superimposing the 2D ^{13}C CSI data onto the axial T2-weighted images was performed to localize the tumor voxels (estimated 68±27% of tumor tissue). Color heatmaps of hyperpolarized [1-^{13}C] α-KG and [1-^{13}C] 2-HG were generated at 20s post start of injection by sinc-based spatial interpolation of the 2D ^{13}C CSI data to the anatomical image resolution using SIVIC.

Post mortem analysis of tumors

One hour after the end of the last hyperpolarized ^{13}C MR experiment, animals (n=5 U87IDHmut, n=4 U87IDHwt) were euthanized. Brains were resected and sectioned in the coronal plane to bisect the tumor.

The posterior sections of the brains were placed in 10% buffered formalin for 24h, and then moved to 70% cold ethanol. The sections were then embedded in paraffin and sectioned in the axial plane. Sections were stained with hematoxylin and eosin (H&E) and immunostained for mutant isocitrate dehydrogenase 1 (IDH1^{R132H}) using a mouse monoclonal anti-IDH1^{R132H} (DIA H09) (Dianova, Miami, FL), at 1:50 dilution. All stained slides were imaged using an Olympus BX41 microscope and Olympus DP72 camera and assessed qualitatively.

The anterior sections of the brains were dissected to isolate the tumor from the normal brain tissue, and tumors were quickly snap-frozen in liquid N_2. Tumor tissues were then extracted using the dual-phase extraction method [57]. After lyophilization, tumor extracts were reconstituted in 400μL D_20 in a 5mm NMR tube and 1D ^{1}H MR spectra were recorded on a on a 14 Tesla Varian INOVA spectrometer (Agilent Technologies, Inc., Palo Alto, CA) using the following parameters: 90-degree *FA*, TR=2s, SW=7194Hz, 20000points, NT=128. *In vivo* 2-HG levels were quantified by peak deconvolution and integration using ACD/ SpecManager™ 9 (Advanced Chemistry Development, Toronto, Canada), correction for saturation and normalization to a TSP reference and to grams of tumor tissue (Cambridge Isotope Laboratories, Andover, MA).

Coil sensitivity in rodents versus humans

In an effort to estimate the achievable SNR of hyperpolarized [1-^{13}C] 2-HG in a patient brain tumor, we needed to account for the decreased sensitivity of the larger coils required for patient studies. To this end, we compared the sensitivity of the rodent coil used in our study to the sensitivity of a human ^{13}C head coil array used for clinical brain imaging (8-channel custom coil array with two 18cm linear panels; four surface coils per panel; rectangular coil element 5×10cm) [58]. A 0.6mL sealed syringe containing 8M [1-^{13}C] urea was positioned in the center of each of the two coils and an identical pulse-acquire sequence was applied to measure the [1-^{13}C] urea signal (90-degree *FA*, NT=64). The decrease in sensitivity in the human coil was assessed by direct comparison of the amplitudes of the [1-^{13}C] urea signal in human vs. rodent coil.

Statistical analysis

All results are expressed as mean ± standard deviation. The unpaired two-tailed Student's *t*-test was used to determine statistical significance of the results, with a p-value less than 0.05 considered as significant.

Supplementary Material

Refer to Web version on PubMed Central for supplementary material.

Acknowledgments

The authors would like to acknowledge Sarah Woods, Dr. Alessia Lodi, Pia Eriksson, Galen Reed and Aaron Robinson. This work was supported by NIH UCSF Brain Tumor SPORE P50 CA097257, NIH R01CA172845, NIH R21CA16154, NIH R01CA154915, NIH P41EB013598, a grant from the UCSF Academic Senate and a fellowship from the American Brain Tumor Association.

References

1. Ward PS, et al. The common feature of leukemia-associated IDH1 and IDH2 mutations is a neomorphic enzyme activity converting alpha-ketoglutarate to 2-hydroxyglutarate. Cancer Cell. 2010; 17:225–234. [PubMed: 20171147]
2. Dang L, et al. Cancer-associated IDH1 mutations produce 2-hydroxyglutarate. Nature. 2009; 462:739–744. [PubMed: 19935646]
3. Mardis ER, et al. Recurring mutations found by sequencing an acute myeloid leukemia genome. The New England journal of medicine. 2009; 361:1058–1066. [PubMed: 19657110]
4. Ohgaki H, Kleihues P. The definition of primary and secondary glioblastoma. Clin Cancer Res. 2013; 19:764–772. [PubMed: 23209033]
5. Yang H, Ye D, Guan KL, Xiong Y. IDH1 and IDH2 mutations in tumorigenesis: mechanistic insights and clinical perspectives. Clin Cancer Res. 2012; 18:5562–5571. [PubMed: 23071358]
6. Losman JA, Kaelin WG Jr. What a difference a hydroxyl makes: mutant IDH, (R)-2-hydroxyglutarate, and cancer. Genes Dev. 2013; 27:836–852. [PubMed: 23630074]
7. Walker EJ, et al. Monoallelic expression determines oncogenic progression and outcome in benign and malignant brain tumors. Cancer research. 2012; 72:636–644. [PubMed: 22144470]
8. Leonardi R, Subramanian C, Jackowski S, Rock CO. Cancer-associated isocitrate dehydrogenase mutations inactivate NADPH-dependent reductive carboxylation. J Biol Chem. 2012; 287:14615–14620. [PubMed: 22442146]
9. Ward PS, et al. The potential for isocitrate dehydrogenase mutations to produce 2-hydroxyglutarate depends on allele specificity and subcellular compartmentalization. J Biol Chem. 2013; 288:3804–3815. [PubMed: 23264629]
10. Turcan S, et al. IDH1 mutation is sufficient to establish the glioma hypermethylator phenotype. Nature. 2012; 483:479–483. [PubMed: 22343889]
11. Xu W, et al. Oncometabolite 2-hydroxyglutarate is a competitive inhibitor of alpha-ketoglutarate-dependent dioxygenases. Cancer Cell. 2011; 19:17–30. [PubMed: 21251613]
12. Huse JT, Phillips HS, Brennan CW. Molecular subclassification of diffuse gliomas: seeing order in the chaos. Glia. 2011; 59:1190–1199. [PubMed: 21446051]
13. Lu C, et al. IDH mutation impairs histone demethylation and results in a block to cell differentiation. Nature. 2012; 483:474–478. [PubMed: 22343901]
14. Popovici-Muller J, et al. Discovery of the First Potent Inhibitors of Mutant IDH1 That Lower Tumor 2-HG in Vivo. Acs Med Chem Lett. 2012; 3:850–855.
15. Rohle D, et al. An Inhibitor of Mutant IDH1 Delays Growth and Promotes Differentiation of Glioma Cells. Science. 2013; 340:626–630. [PubMed: 23558169]
16. Nelson SJ. Assessment of therapeutic response and treatment planning for brain tumors using metabolic and physiological MRI. NMR in biomedicine. 2011; 24:734–749. [PubMed: 21538632]

17. Julia-Sape M, et al. Prospective diagnostic performance evaluation of single-voxel 1H MRS for typing and grading of brain tumours. NMR in biomedicine. 2012; 25:661–673. [PubMed: 21954036]
18. Andronesi OC, et al. Detection of 2-hydroxyglutarate in IDH-mutated glioma patients by in vivo spectral-editing and 2D correlation magnetic resonance spectroscopy. Sci Transl Med. 2012; 4:116ra114.
19. Choi C, et al. 2-hydroxyglutarate detection by magnetic resonance spectroscopy in IDH-mutated patients with gliomas. Nat Med. 2012; 18:624–629. [PubMed: 22281806]
20. Pope WB, et al. Non-invasive detection of 2-hydroxyglutarate and other metabolites in IDH1 mutant glioma patients using magnetic resonance spectroscopy. J Neurooncol. 2012; 107:197–205. [PubMed: 22015945]
21. Esmaeili M, Vettukattil R, Bathen TF. 2-hydroxyglutarate as a magnetic resonance biomarker for glioma subtyping. Transl Oncol. 2013; 6:92–98. [PubMed: 23544162]
22. Lazovic J, et al. Detection of 2-hydroxyglutaric acid in vivo by proton magnetic resonance spectroscopy in U87 glioma cells overexpressing isocitrate dehydrogenase-1 mutation. Neuro Oncol. 2012; 14:1465–1472. [PubMed: 23090985]
23. Chaumeil, MM., et al. In vivo comparison of total and hyperpolarized lactate levels assessed by localized 1H MRS and hyperpolarized 13C MRSI in glioblastoma models at 14.1Tesla. International Society of Magnetic Resonance in Medicine; Melbourne, Australia. 2012.
24. Kalinina J, et al. Detection of “oncometabolite” 2-hydroxyglutarate by magnetic resonance analysis as a biomarker of IDH1/2 mutations in glioma. J Mol Med (Berl). 2012; 90:1161–1171. [PubMed: 22426639]
25. Elkhaled A, et al. Magnetic resonance of 2-hydroxyglutarate in IDH1-mutated low-grade gliomas. Sci Transl Med. 2012; 4:116ra115.
26. Ardenkjaer-Larsen JH, et al. Increase in signal-to-noise ratio of > 10,000 times in liquid-state NMR. Proc Natl Acad Sci U S A. 2003; 100:10158–10163. [PubMed: 12930897]
27. Kurhanewicz J, et al. Analysis of cancer metabolism by imaging hyperpolarized nuclei: prospects for translation to clinical research. Neoplasia. 2011; 13:81–97. [PubMed: 21403835]
28. Day SE, et al. Detecting tumor response to treatment using hyperpolarized 13C magnetic resonance imaging and spectroscopy. Nat Med. 2007; 13:1382–1387. [PubMed: 17965722]
29. Ward CS, et al. Noninvasive detection of target modulation following phosphatidylinositol 3-kinase inhibition using hyperpolarized 13C magnetic resonance spectroscopy. Cancer research. 2010; 70:1296–1305. [PubMed: 20145128]
30. Park I, et al. Detection of early response to temozolomide treatment in brain tumors using hyperpolarized 13C MR metabolic imaging. Journal of magnetic resonance imaging : JMRI. 2011; 33:1284–1290. [PubMed: 21590996]
31. Chaumeil MM, et al. Hyperpolarized 13C MR spectroscopic imaging can be used to monitor Everolimus treatment in vivo in an orthotopic rodent model of glioblastoma. Neuroimage. 2012; 59:193–201. [PubMed: 21807103]
32. Day SE, et al. Detecting response of rat C6 glioma tumors to radiotherapy using hyperpolarized [1-13C]pyruvate and 13C magnetic resonance spectroscopic imaging. Magnetic resonance in medicine. 2011; 65:557–563. [PubMed: 21264939]
33. Nelson SJ, et al. Metabolic Imaging of Patients with Prostate Cancer Using Hyperpolarized [1-13C]Pyruvate. Sci Transl Med. 2013
34. Larson PE, et al. Multiband excitation pulses for hyperpolarized 13C dynamic chemical-shift imaging. J Magn Reson. 2008; 194:121–127. [PubMed: 18619875]
35. Xing Y, Reed GD, Pauly JM, Kerr AB, Larson PEZ. Optimal Variable Flip Angle Schemes For Multi-Band Dynamic Acquisition Of Hyperpolarized 13C MRSI. J Magn Reson. 2013 In press.
36. Cunningham CH, et al. Double spin-echo sequence for rapid spectroscopic imaging of hyperpolarized 13C. J Magn Reson. 2007; 187:357–362. [PubMed: 17562376]
37. Larson PE, et al. Investigation of tumor hyperpolarized [1-13C]-pyruvate dynamics using time-resolved multiband RF excitation echo-planar MRSI. Magnetic resonance in medicine. 2010; 63:582–591. [PubMed: 20187172]

38. Kazan SM, et al. Kinetic modeling of hyperpolarized (13) C pyruvate metabolism in tumors using a measured arterial input function. Magnetic resonance in medicine. 2012 Epub ahead of print.
39. Chen AP, et al. Hyperpolarized C-13 spectroscopic imaging of the TRAMP mouse at 3T-initial experience. Magnetic resonance in medicine. 2007; 58:1099–1106. [PubMed: 17969006]
40. Chen AP, et al. Feasibility of using hyperpolarized [1-13C]lactate as a substrate for in vivo metabolic 13C MRSI studies. Magn Reson Imaging. 2008; 26:721–726. [PubMed: 18479878]
41. Hu S, et al. In vivo measurement of normal rat intracellular pyruvate and lactate levels after injection of hyperpolarized [1-(13)C]alanine. Magn Reson Imaging. 2011; 29:1035–1040. [PubMed: 21855243]
42. Ardenkjaer-Larsen JH, et al. Dynamic nuclear polarization polarizer for sterile use intent. NMR in biomedicine. 2011; 24:927–932. [PubMed: 21416540]
43. Batel M, et al. A multi-sample 94 GHz dissolution dynamic-nuclear-polarization system. J Magn Reson. 2012; 214:166–174. [PubMed: 22142831]
44. Luchman HA, et al. An in vivo patient-derived model of endogenous IDH1-mutant glioma. Neuro Oncol. 2012; 14:184–191. [PubMed: 22166263]
45. MacKenzie ED, et al. Cell-permeating alpha-ketoglutarate derivatives alleviate pseudohypoxia in succinate dehydrogenase-deficient cells. Mol Cell Biol. 2007; 27:3282–3289. [PubMed: 17325041]
46. Shank RP, Bennett DJ. 2-Oxoglutarate transport: a potential mechanism for regulating glutamate and tricarboxylic acid cycle intermediates in neurons. Neurochem Res. 1993; 18:401–410. [PubMed: 8097291]
47. Smolkova K, Jezek P. The Role of Mitochondrial NADPH-Dependent Isocitrate Dehydrogenase in Cancer Cells. Int J Cell Biol. 2012; 2012:273947. [PubMed: 22675360]
48. Hurd RE, et al. Metabolic imaging in the anesthetized rat brain using hyperpolarized [1-13C] pyruvate and [1-13C] ethyl pyruvate. Magnetic resonance in medicine. 2010; 63:1137–1143. [PubMed: 20432284]
49. Park I, et al. Hyperpolarized 13C magnetic resonance metabolic imaging: application to brain tumors. Neuro Oncol. 2010; 12:133–144. [PubMed: 20150380]
50. Bhattacharya R, Gujar N, Singh P, Rao P, Vijayaraghavan R. Toxicity of alpha-ketoglutarate following 14-days repeated oral administration in Wistar rats. Cell Mol Biol (Noisy-le-grand). 2011; 57(Suppl):OL1543–1549. [PubMed: 21791173]
51. Marjanska M, et al. In vivo 13C spectroscopy in the rat brain using hyperpolarized [1-(13)C]pyruvate and [2-(13)C]pyruvate. J Magn Reson. 2010; 206:210–218. [PubMed: 20685141]
52. Gallagher FA, et al. Production of hyperpolarized [1,4-13C2]malate from [1,4-13C2]fumarate is a marker of cell necrosis and treatment response in tumors. Proc Natl Acad Sci U S A. 2009; 106:19801–19806. [PubMed: 19903889]
53. Golman K, Zandt RI, Lerche M, Pehrson R, Ardenkjaer-Larsen JH. Metabolic imaging by hyperpolarized 13C magnetic resonance imaging for in vivo tumor diagnosis. Cancer research. 2006; 66:10855–10860. [PubMed: 17108122]
54. Fatania HR, al-Nassar KE, Thomas N. Chemical modification of rat liver cytosolic NADP(+)-linked isocitrate dehydrogenase by N-ethylmaleimide. Evidence for essential sulphydryl groups. FEBS Lett. 1993; 322:245–248. [PubMed: 8486157]
55. Yan H, et al. IDH1 and IDH2 mutations in gliomas. N Engl J Med. 2009; 360:765–773. [PubMed: 19228619]
56. Ozawa T, et al. Growth of human glioblastomas as xenografts in the brains of athymic rats. In Vivo. 2002; 16:55–60. [PubMed: 11980362]
57. Brandes AH, Ward CS, Ronen SM. 17-allyamino-17-demethoxygeldanamycin treatment results in a magnetic resonance spectroscopy-detectable elevation in choline-containing metabolites associated with increased expression of choline transporter SLC44A1 and phospholipase A2. Breast Cancer Res. 2010; 12:R84. [PubMed: 20946630]
58. Ohliger MA, et al. Combined parallel and partial fourier MR reconstruction for accelerated 8-channel hyperpolarized carbon-13 in vivo magnetic resonance spectroscopic imaging (MRSI). Journal of magnetic resonance imaging : JMRI. 2013

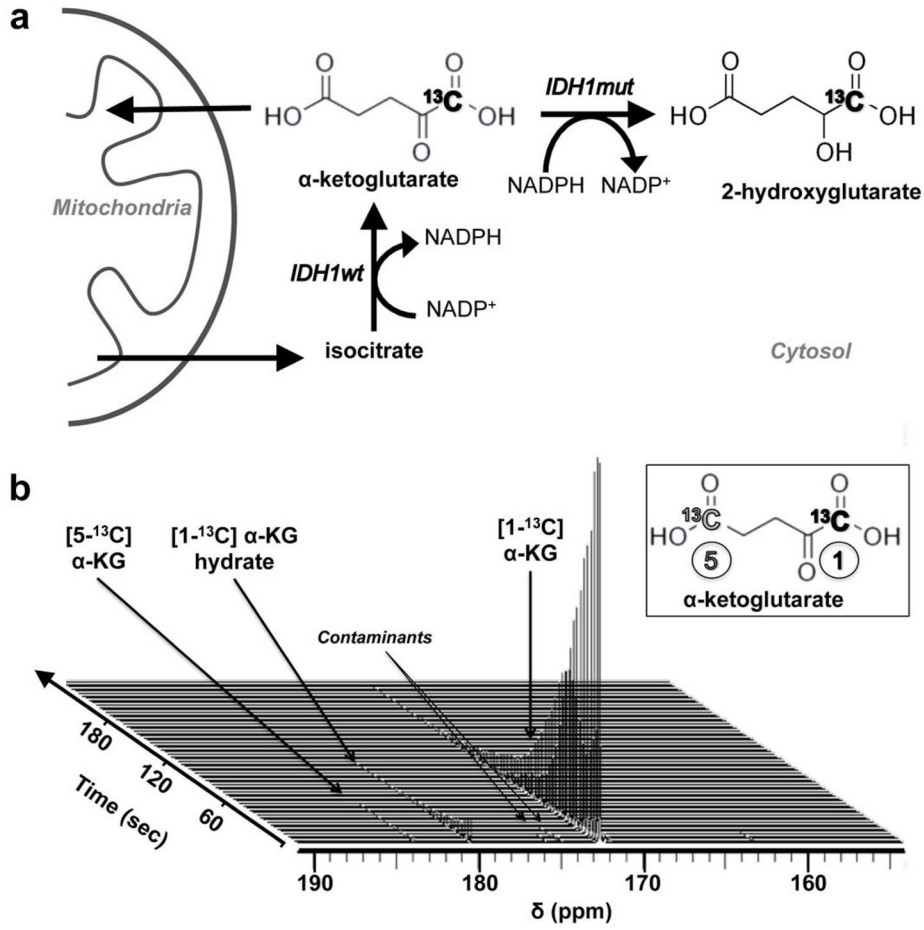

Figure 1. [1-^{13}C] α-KG is a biologically relevant DNP probe

(a) Schematic of reactions catalyzed by wild-type IDH1 (*IDH1wt*) and mutant IDH1 (*IDH1mut*), and associated [1-^{13}C] α-KG metabolism. The ^{13}C label at the C1 position of α-KG is highlighted in bold. **(b)** Stack plot of ^{13}C MR spectra of hyperpolarized [1-^{13}C] α-KG in solution acquired at 11.7 Tesla, and showing decay of the hyperpolarized signals (temporal resolution 3s, polarization level 17%). Hyperpolarized [1-^{13}C] α-KG ($\delta_{C1\text{-}\alpha KG}$=172.6ppm, insert black), hyperpolarized [1-^{13}C] α-KG hydrate ($\delta_{\alpha KG\text{-}H}$ =180.9ppm) and hyperpolarized [5-^{13}C] α-KG ($\delta_{C5\text{-}\alpha KG}$ =184ppm, insert grey) are detectable.

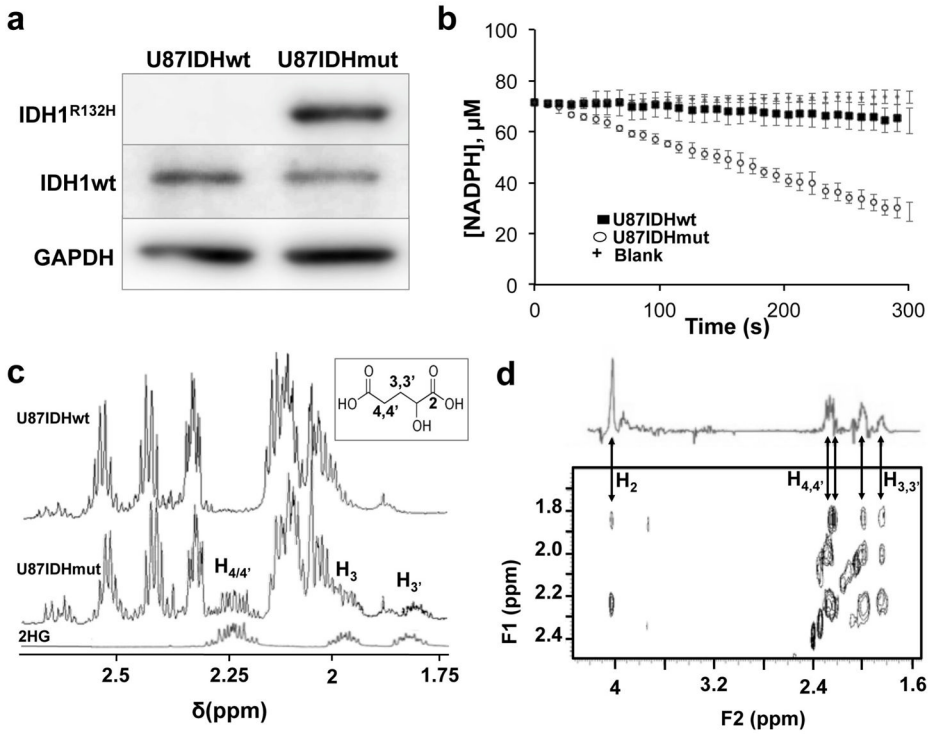

Figure 2. Mutant IDH1 cells exhibit elevated enzyme activity and 2-HG levels

(a) Western blotting for wild-type IDH1 (IDH1wt, 46kDa) and mutant IDH1 ($IDH1^{R132H}$, 46kDa) isoforms in U87IDHmut and U87IDHwt cells (GAPDH (40.2kDa) was used as a loading control; see Supplementary Figure S1 for full blots). **(b)** Spectrophotometric assay of mutant IDH1 activity in U87IDHwt (■) and U87IDHmut (○) cells, monitoring changes in NADPH absorption over time at 340 nm, compared to buffer blank (+). **(c)** ^{1}H spectra of pure 2-HG (bottom), U87IDHwt cell lysate (top) and U87IDHmut cell lysate (middle). Insert shows the structure of 2-HG and annotated protons detected in the spectrum. **(d)** Zoomed view of 2D ^{1}H TOCSY of a U87IDHmut cell lysate acquired at 14 Tesla, illustrating the cross peaks characteristic of 2-HG (H_2=4.00ppm; $H_{3,3'}$=1.85/2.00ppm; $H_{4,4'}$=2.25ppm). A projection representing the sum of all slices containing the 2-HG spin system is shown on top of the TOCSY box.

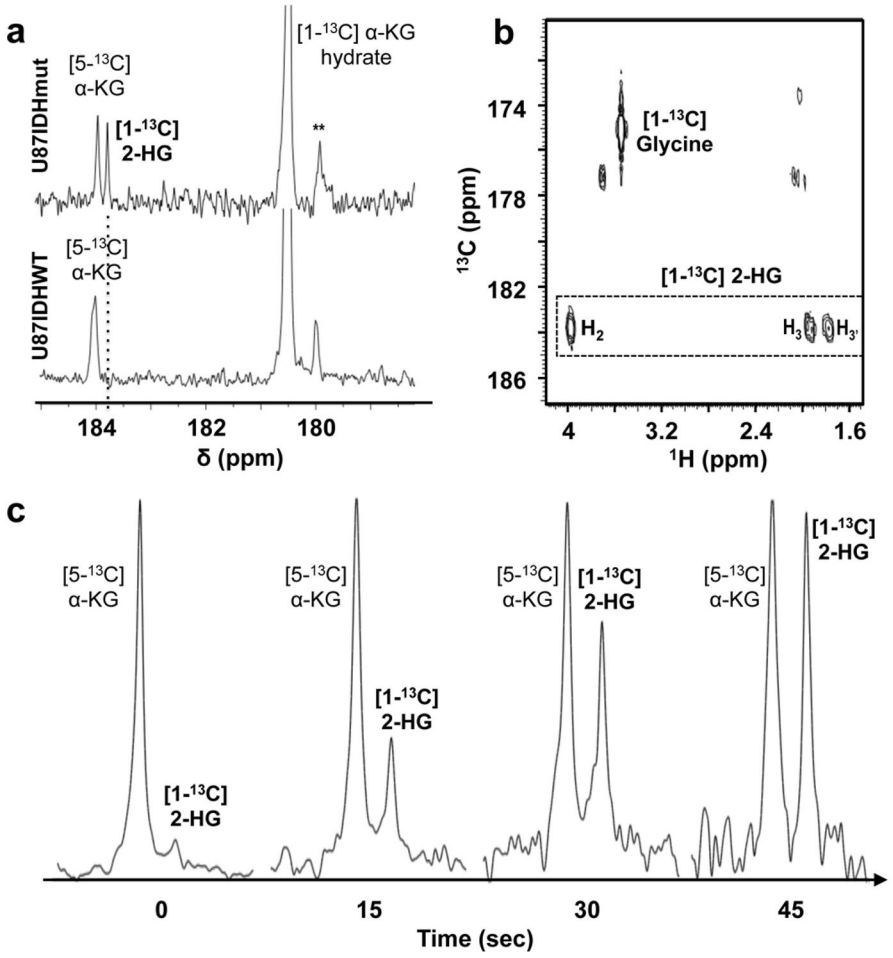

Figure 3. Hyperpolarized 2-HG production is detected in mutant IDH1 cell lysates

(a) ^{13}C MR spectra acquired 45s after injection of hyperpolarized [1-^{13}C] α-KG in U87IDHmut cell lysate (top) and U87IDHwt cell lysate (bottom) (absolute intensities; * contaminant originating from the α-KG preparation). (**b**) gHMBC spectra of the same U87IDHmut lysates acquired at 14 Tesla, confirming the production of [1-^{13}C] 2-HG from [1-^{13}C] α-KG. The ^{1}H-^{13}C cross peaks of [1-^{13}C] 2-HG (dotted box), confirm the [1-^{13}C] 2-HG assignment at 183.9ppm. Note: [1-^{13}C] glycine was used as an external reference. **(c)** Temporal evolution of [1-^{13}C] 2-HG in U87IDHmut cell lysate normalized to [5-^{13}C] α-KG peak intensity, showing build-up of hyperpolarized [1-^{13}C] 2-HG.

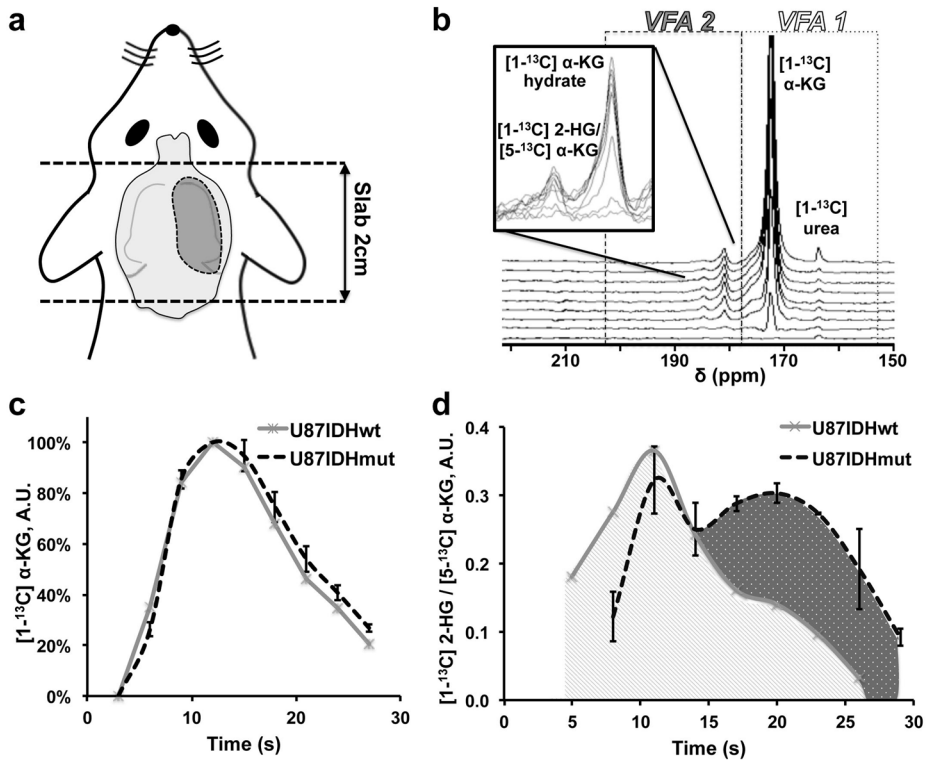

Figure 4. Hyperpolarized 2-HG can be detected *in vivo* in mutant IDH1 tumors

(a) Schematic of axial slab used for *in vivo* dynamic ^{13}C MR experiments. The 2cm slab was positioned to include the whole tumor while minimizing contamination from neck and nose blood vessels. **(b)** Stack plot of *in vivo* dynamic ^{13}C MR spectra acquired from a 2cm slab following injection of hyperpolarized [1-^{13}C] α-KG in a tumor-bearing U87IDHmut rat (temporal resolution 5s; lb=20Hz). A variable flip angle scheme (*VFA1*/*VFA2*, see **Methods**) was used in order to improve the signal of hyperpolarized [1-^{13}C] 2-HG. Signals from hyperpolarized [1-^{13}C] α-KG ($\delta_{C1\text{-}\alpha KG}$ =172.6ppm), hyperpolarized [1-^{13}C] α-KG hydrate ($\delta_{\alpha KG\text{-}H}$ =180.9ppm) and the resonance of hyperpolarized [1-^{13}C] 2-HG/[5-^{13}C] α-KG (δ =184ppm) are visible. **(c)** Integral of hyperpolarized [1-^{13}C] α-KG as a function of time after its intravenous injection as measured from slab dynamic ^{13}C spectra acquired in U87IDHmut (black, n=3) and U87IDHwt (grey, n=2) tumor-bearing animals (error bars: ± standard deviation of the mean). **(d)** Integral of the 184ppm resonance ([1-^{13}C] 2-HG/ [5-^{13}C] α-KG) as measured from slab dynamic ^{13}C spectra acquired in U87IDHmut (black, n=3) and U87IDHwt (grey, n=2) tumor-bearing animals (error bars: ± standard deviation of the mean). The bimodal temporal evolution of the composite resonance in U87IDHmut suggests metabolic production of hyperpolarized [1-^{13}C] 2-HG.

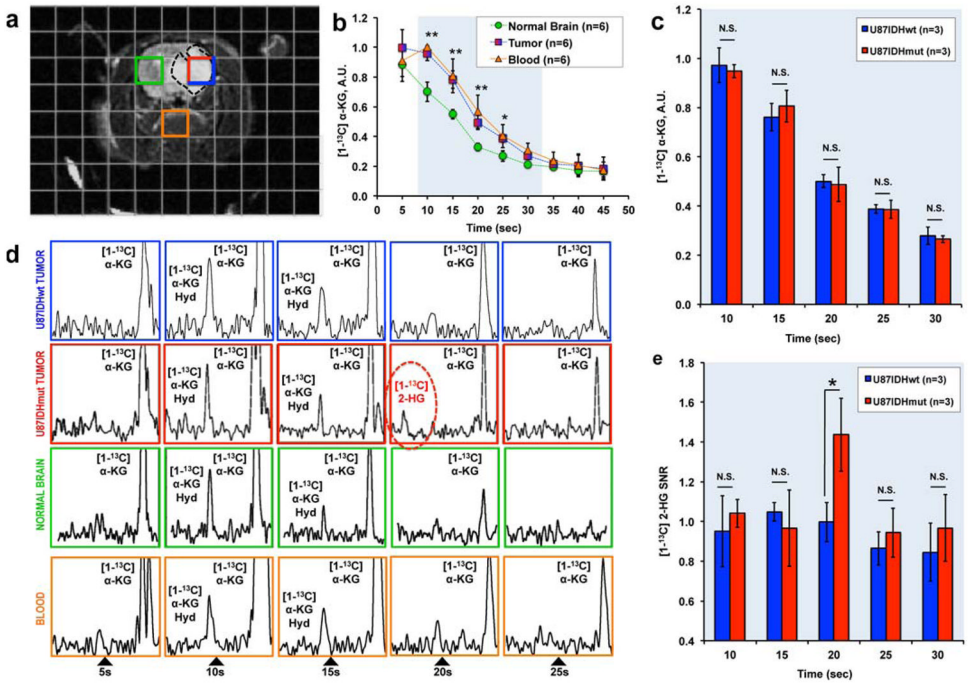

Figure 5. Hyperpolarized α-KG is delivered and converted to 2-HG *in situ*

(a) T2-weighted anatomical MR image of U87IDHmut tumor-bearing animal overlaid with the grid used for 2D ^{13}C CSI acquisition (red/blue: tumor voxel; orange: blood voxel; green: normal brain voxel). **(b)** Time courses of hyperpolarized [1-^{13}C] α-KG measured in tumor voxels (red/blue - n=6, including n=3 U87IDHmut and n=3 U87IDHwt), in normal brain voxels (green - n=6), and in blood-containing voxels centered on the basal artery (orange - n=6) (error bars: ± standard deviation of the mean). Significantly higher levels of hyperpolarized [1-^{13}C] α-KG were observed in the tumor voxels as compared to normal brain (Unpaired Student *t*-test: ***p<0.005* at 10s, 15s, 20s and 25s; **p<0.05* at 30s). **(c)** Levels of hyperpolarized [1-^{13}C] α-KG measured in U87IDHwt (blue, n=3) and U87IDHmut (red, n=3) tumor voxels at 10s, 15s, 20s, 25s and 30s (error bars: ± standard deviation of the mean). No significant difference was observed at any time point. **(d)** Hyperpolarized ^{13}C MR spectra from one U87IDHwt tumor voxel (blue), one U87IDHmut tumor voxel (red), one normal brain voxel (green), and one blood voxel (orange) showing the temporal evolution of metabolites (no averaging performed; all spectra normalized to noise level). A resonance at 184ppm was observed at 20s post injection of hyperpolarized [1-^{13}C] α-KG only in the IDH1 mutant tumor voxel. (Note: the data presented from the U87IDHmut tumor, blood, and normal brain voxels, correspond to the U87IDHmut animal presented in Figure 5a; the data from the U87IDHwt tumor are from an animal for which the MR image is not shown) (Hyd: hydrate) **(e)** SNR of the 184ppm resonance measured in U87IDHwt (blue) and U87IDHmut (red) tumor voxels at 10s, 15s, 20s, 25s and 30s (error bars: ± standard deviation of the mean). A significant difference was found at 20s post injection: SNR=1.4±0.2 in U87IDHmut tumors (n=3) *vs.* SNR=1.1±0.1 in U87IDHwt tumors (n=3, Unpaired Student *t*-test: **p<0.05*) consistent with this resonance corresponding to [1-^{13}C] 2-HG.

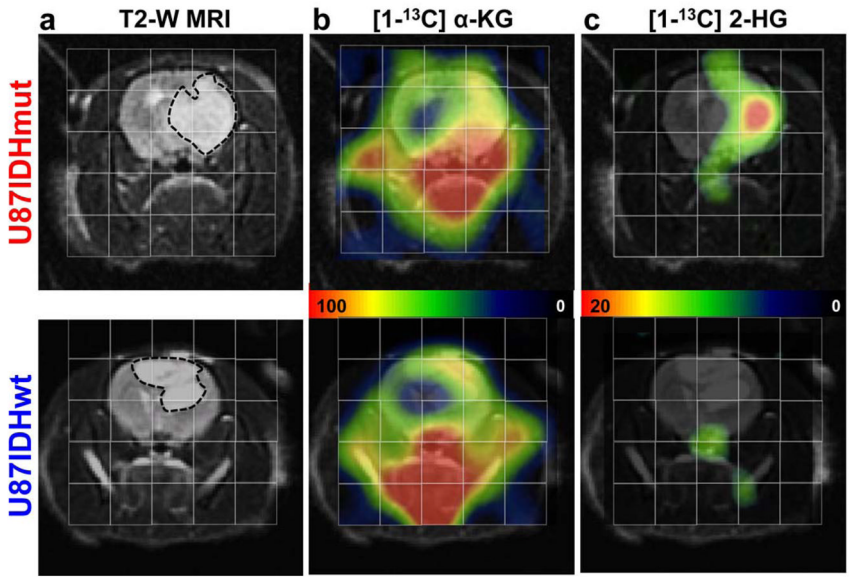

Figure 6. Hyperpolarized 2-HG is detected only in mutant IDH1 tumors

(a) T2-weighted anatomical MR image of the head of a U87IDHmut (top) and a U87IDHwt (bottom) tumor-bearing animal overlaid with the grid used for 2D ^{13}C CSI acquisition. The tumors appear as hyperintense regions. **(b)** Corresponding heatmaps of hyperpolarized [1-^{13}C] α-KG at 20s post injection. **(c)** Corresponding heatmaps of hyperpolarized [1-^{13}C] 2-HG at 20s post injection, illustrating the presence of this metabolite in IDH1 mutant tumors only.

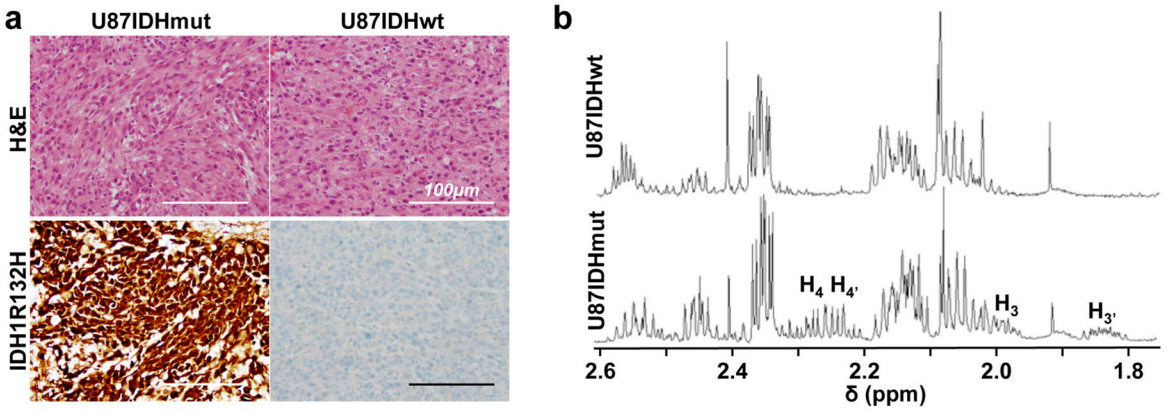

Figure 7. *Post mortem* analysis confirms the presence of mutant IDH1 and 2-HG

(a) U87IDHmut (left) and U87IDHwt (right) tumors had a similar histologic appearance and were densely cellular on hematoxylin and eosin staining (H&E, top row). Immunostaining for mutant IDH1 ($IDH1^{R132H}$, bottom row) demonstrated robust, diffuse positivity in U87IDHmut (left) tumors and no positive staining in U87IDHwt (right) tumors (magnification ×200, scale bar 100μm). (**b**) ^{1}H MR spectrum of U87IDHwt (top) and U87IDHmut (bottom) tumor lysates acquired at 14 Tesla. The multiplets characteristic of 2-HG can be seen in the U87IDHmut spectrum, not in the U87IDHwt ($H_{3'}$=1.85ppm; H_3=2.00ppm; $H_{4,4'}$=2.25ppm; see Figure 2 for proton assignments). The level of 2-HG in U87IDHmut tumor extracts was 9.8±1.6 μmol per gram of tumor (n=3).

Table 1

T_1 relaxation times of ^{13}C-labeled compounds of interest

	Relaxation time T_1 (sec)	
	3 Tesla	**11.7 Tesla**
[1-^{13}C] α-Ketoglutarate	52 ± 4	19 ± 3
[1-^{13}C] α-Ketoglutarate hydrate	54 ± 2	16 ± 4
[5-^{13}C] α-Ketoglutarate	41 ± 2	18 ± 4
[1-^{13}C] 2-hydroxyglutarate	26*	17*

In vitro relaxation times measured in solution at 3 Tesla and 11.7 Tesla (37°C, pH=7.5±0.1, n=3 per measurement, except for 2-HG: *$n=1$).